Speckle noise suppression of reconstructed image in digital holography based on BM3D improved convolutional neural network

Yuan Chen[1,3,*], Yuhui Fan[2], Guangming Zhang[4], Quan Wang[2], Sitian Li[2], Zhongyang Wang[2], Ming Dong[2,3]

1College of Sciences, Xi'an University of Science and Technology, Xi'an, Shaanxi, 710054, China

2College of Mechanical Engineering, Xi'an University of Science and Technology, Xi'an, Shaanxi,710054, China

3Shaanxi Key Laboratory of Mine Electromechanical Equipment Intelligent Detection and Control, Xi'an University of Science and Technology, Xi'an, Shaanxi, 710054, China

4 General Engineering Research Institute, School of Engineering, Faculty of Engineering and Technology, Liverpool John Moores University, Byrom Street, L3 3AF, United Kingdom

**Email: chenyuan1030@126.com*

Abstract: In digital holographic measurement, when light waves pass through inhomogeneous media or surfaces, speckle noise is generated, resulting in random, granular light and dark spots in the hologram, which greatly reduces the image quality. Therefore, in order to improve the image quality of holographic reconstruction, a noise reduction method based on BM3D improved convolutional neural network (CNN) is proposed in this paper. Firstly, the similarity and important statistical information between blocks can be obtained by using BM3D. Then, the denoising convolutional neural network (DnCNN) is used to learn the relationship between the noise of a large number of samples and the noise image, and further purify the image to retain the details for a better denoising effect. Finally, a reflective off-axis digital holographic optical path system is constructed to collect the holograms of the test samples, and the reconstructed images are obtained by the Fresnel diffraction method to constitute a dataset with the simulated holographic reconstructed images to validate the proposed method in this paper, compared to the other methods, such as DnCNN, convolutional blind denoising network (CBDNet), BM3D and Wiener filtering. The experimental results of qualitative and quantitative analysis show that the proposed method combines the advantages of traditional algorithms and deep learning, significantly enhances the robustness of the system, optimizes the denoising performance, and preserves the details of the reconstructed image to the greatest extent.

Keywords: digital holography; noise suppression; convolutional neural network; BM3D

1 Introduction

Digital holography (DH) is a technology that uses computer technology and optical principles to generate and reproduce the contours of three-dimensional objects. It generates and records the interference between the transmitted or reflected light of an object and the reference light, then processes and reconstructs the hologram using a computer, finally obtaining a three-dimensional image of the object. Due to its good performance in three-dimensional data measurement, it has been widely used in various fields, such as holographic data storage systems [1], biological cell observation [2], and holographic microscope measurement, et al. [3]. The emergence of lasers laid a foundation for the development of holography [4]. The high coherence of lasers allows DH to record and reconstruct the phase information of an object, and the high brightness and directivity of the laser also help to improve the quality and stability of DH, which can result in high-resolution images [5][6]. However, when the laser beam passes through an inhomogeneous medium, light interference occurs, causing irregular fluctuations in the intensity distribution of the light field and forming randomly distributed speckle noise. The speckle noise in the hologram belongs to the multiplicative noise and is distributed independently with the original image, which reduces the image quality and causes the

measurement errors, limiting the application of DH in the field of microstructure measurement [7]. At present, speckle noise suppression methods mainly include: low-coherence light source illumination method, multiple hologram superposition averaging method and digital image processing method [8].

The low-coherence light source illumination method reduces the speckle noise from the root by reducing the spatial coherence of the light source. Dubois et al. [9] changed the spatial coherence state of the sample illumination by varying the spot size of the laser beam on a rotating ground glass, and improved the image quality. Gong et al. [10] proposed a partially coherent optical DH technique using a light-emitting diode as the light source, which eliminated the speckle noise caused by the laser light source and the parasitic interference noise introduced by the optics, and improved the signal-to-noise ratio of the reconstructed image.

The multiple hologram superposition averaging method is to record multiple holograms containing uncorrelated noise patterns using different optical methods and reduce the coherent noise by using the superposition averaging effect. Joseph et al. [11] proposed a new method to record the digital holograms under incoherent illumination conditions by propagating through a diffractive optical element, recording three holograms consecutively, and then superimposing the three holograms with different phase factors to obtain a complex-valued Fresnel hologram. The reconstructed image well revealed the three-dimensional nature of the object. Chen et al. [12] proposed a neighborhood filter based on multiple sub-reconstructed images, which used the correlation between different positions of multiple sub-holograms to calculate the weights, and used the weighted sum of neighboring pixel values as the denoising value. The experimental results showed that this method has a good performance on noise reduction.

Compared with the above two methods, the digital image processing method does not require harsh experimental conditions and is more suitable for the dynamic characteristics of digital holography. It has a flexible process that can be optimized for different images. Bianco et al. [13] proposed a fast non-Bayesian denoising method by numerically synthesizing a moving diffuser using only a single hologram and providing multiple uncorrelated reconstructed images using a random complementary resampling mask. Experimental results demonstrated that the incoherent noise was reduced while maintaining the image resolution. Chen et al. [14] applied bidimensional empirical mode decomposition (BEMD) to decompose the reconstructed image into a series of two-dimensional intrinsic mode function components with different frequencies, and then selected a certain number of two-dimensional intrinsic mode function components for noise reduction using the variational method. The improved particle swarm optimization algorithm was adopted to automatically select the key parameters of the proposed method, which further improved its noise reduction performance.

The traditional speckle noise reduction algorithms have some shortcomings in dealing with complex speckle noise, preserving image details, computational efficiency and parameter selection. While neural network has a powerful computational ability and image feature detection ability, which can learn and identify noise patterns through its powerful feature learning ability to achieve accurate denoising while preserving image details, demonstrating good noise reduction performance and wide practicability. Therefore, a number of deep learning-based noise reduction methods have been reported in recent years, which can better remove speckle noise and preserve image details. Choi et al. [15] proposed a cycle-consistent deep neural network that used unpaired images for training to learn the conversion between clean and noisy refractive index tomography images, and achieved coherent noise removal in three-dimensional quantitative phase imaging. Chen et al. [16] presented a noise reduction algorithm based on a wavelet domain residual network, which can learn the noise in the wavelet

domain to directly reduce the noise of the reconstructed image, and trained on a dataset synthesized from the direct reconstruction image of the lensless in-line holographic microscope and the high-resolution real image collected by the microscope. The results showed that the image resolution and contrast were significantly improved compared to the traditional reconstruction methods. To obtain clearer phase information, Fang et al. [17] developed a deep learning-based speckle denoising algorithm using conditional generative adversarial networks. Two sub-networks composed of U-Net and DenseNet layer structures were used to monitor network learning quality and denoising, respectively. Experiments showed that the accuracy of subsequent phase extraction was improved.

The above-mentioned models have a complex structure, are difficult to train, require high computational resources, and are not suitable for situations with limited resources. Compared to other neural networks for image noise reduction, DnCNN adopts a convolutional neural network structure and an end-to-end training method. This allows it to better learn the complex noise distributions and features in the image, resulting in a direct mapping from the original image to the noise reduction image. The DnCNN simplifies the process of noise reduction, improving the efficiency and performance of network [18]. Additionally, it is highly robust in processing various types of noise and incorporates a residual learning mechanism that exhibits a strong generalization capability [19]. Thus, in this paper, based on the residual learning and batch normalized convolutional neural network algorithm [20], we propose a BM3D-based improved convolutional neural network to achieve speckle noise suppression of reconstructed images in DH. The reflective off-axis digital holographic optical path system is used to collect the holograms of test samples to carry out experimental research, and the effectiveness of the proposed method is verified by comparing the denoising results with those of several commonly used methods.

2 Principle and Method

2.1 Digital holography

Digital holographic imaging includes two steps: holographic recording and diffraction reconstruction [21]. When the object light interferes with the reference light, the interference pattern is recorded as a hologram. The basic principle of digital holographic recording is shown in Fig.1, where $R(x, y)$ is the reference light, $O(x, y)$ is the object light, d is the diffraction distance, the coordinate xy is the CCD window, and $x_i y_i$ is the holographic reconstruction plane. Digital holographic microscopic measurement can be achieved by pre-amplifying the objective light with the microscopic objective lens before interfering, and using the amplified image output from the objective lens as the new objective light. Given the reference light $R(x, y)$ and the object light $O(x, y)$, the intensity distribution $I(x, y)$ of the hologram can be expressed as:

$$I(x,y) = |R(x,y) + O(x,y)|^2 = |O(x,y)|^2 + |R(x,y)|^2 + O(x,y)R^*(x,y) + R(x,y)O^*(x,y) \quad (1)$$

where $R^*(x, y)$ is the conjugate of the reference light, $O^*(x, y)$ is the conjugate of object light, $|O(x,y)|^2 + |R(x,y)|^2$ is the zero-order of diffraction, $O(x,y)R^*(x,y)$ and $R(x,y)O^*(x,y)$ are +1-order image (real image) and -1-order image (virtual image), respectively.

Taking the hologram on the recording plane as the complex amplitude of the optical wave field on the initial plane, the amplitude (x_i, y_i) of the reconstructed image plane at the diffraction distance d can be calculated by Fresnel diffraction method, which can be expressed as:

$$U(x,y) = \frac{1}{j\lambda d} exp\left(j\frac{2\pi}{\lambda}d\right) exp\left[j\frac{\pi}{\lambda d}(x^2+y^2)\right] \mathcal{F}\left\{u(x_0,y_0) exp\left[j\frac{\pi}{\lambda d}(x_0^2+y_0^2)\right]\right\} \quad (2)$$

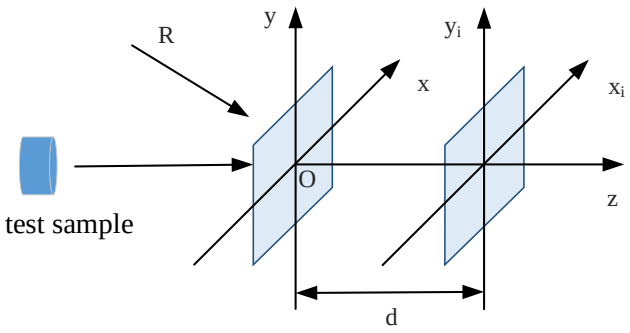

Fig.1. The basic principle diagram of DH.

where λ represents the wavelength of the illumination light, d is the propagation distance, $u(x_0, y_0)$ is the complex amplitude distribution of the diffraction plane light field, and $\mathcal{F}\{\cdot\}$ is the Fast Fourier Transform.

2.2 Speckle noise model

When the laser beam passes through the inhomogeneous medium, due to the inhomogeneity of the internal density and refractive index of the medium, the laser signal will appear the phenomenon of 'random walk', i.e. the propagation path of the light wave deviates from the straight line and becomes random and irregular, which leads to the complex interference effect of light waves inside the medium, as shown in Fig.2. Both the enhancement of coherence Fig. 2 (a) and the weakening of cancellation Fig. 2 (b) lead to the irregular fluctuation of the intensity distribution.

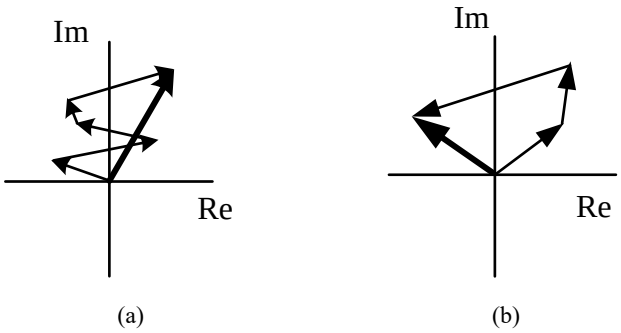

Fig. 2. Schematic diagram of the interference effect of light waves. (a) long interference; (b) destructive interference.

These irregular fluctuations are accurately captured during digital holographic imaging, resulting in a random distribution of speckle noise, which can be expressed as [22]:

$$g(n,m) = f(n,m) \cdot u(n,m) + v(n,m) \tag{3}$$

where (n,m) is the coordinate position in the image, n and m are the horizontal and vertical ordinates, $f(n,m)$ is the value of the original noise-free hologram at the coordinates (n,m), that is, the image that is to be recovered in the ideal state, $u(n,m)$ and $v(n,m)$ are the multiplicative and additive noise components independent of the original image distribution, respectively, and $g(n,m)$ is the image contaminated by speckle noise. Since the speckle noise is composed of multiplicative and additive components, it is difficult for optical holography and traditional image denoising methods to effectively suppress the speckle noise, and the speckle noise varies with the surface condition of the measured object [23]. It is difficult to estimate the speckle noise component of the holograms, which complicates the recovery of the holograms.

2.3 DnCNN

Traditional denoising networks are to output denoising data by optimizing the loss function between

the noise-free data and the output of the denoising network given noisy data. While DnCNN uses a convolutional neural network structure, the output is a prediction of the noise by learning the noise distribution and features in the image. Then, the original noisy image is subjected to pixel-by-pixel phase reduction with the predicted noise image to obtain the denoised image. The denoising principle of the DnCNN model is shown in Fig.3.

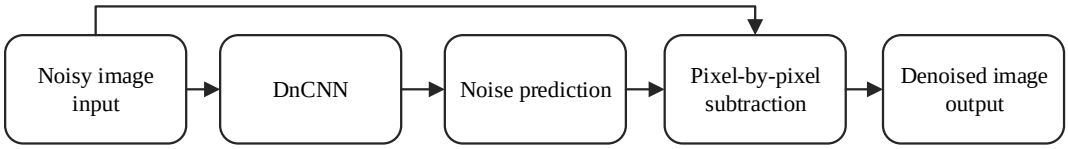

Fig.3. Schematic diagram of the DnCNN model.

The DnCNN model incorporates batch normalization and residual learning, resulting in a significant improvement in the denoising effect. Residual learning makes it easier for the network to learn the subtle features in the image without directly predicting the noise-free image. It only needs to predict a small part of the noise in the image, which reduces the prediction difficulty of the model to some extent, and improves the performance and generalization ability of network. During network training, the input data distribution of each layer is affected by the parameter updates of the previous layer. Batch Normalization (BN) keeps the input of each layer within a small range and then feeds them into the next layer of the network. Because normalization is performed for each training, which makes the network more stable and easier to train, while the network converges faster.

3 Improved Convolutional Neural Network Based on BM3D

3.1 Network Architecture

BM3D performs image noise reduction using block matching and 3D filtering. Firstly, the input image is divided into overlapping square blocks of equal size. For each block, the BM3D algorithm searches for the most similar block in the local neighborhood to complete the block matching, then performs a 3D transformation on the similar blocks, and finally reaggregates the 3D filtered blocks into the image to generate the denoised image.

The principle of the proposed in this paper is described as follows: the input original image is divided into overlapping blocks, and then block matching, 3D transformation and block preprocessing are performed, which aims to capture the similarity and important statistical information between blocks using the BM3D algorithm, and perform preliminary noise reduction processing on the image; then, the BM3D preprocessed image blocks are input to the improved DnCNN to achieve deeper denoising of the images by learning the relationship between the noise and the noisy images from a large number of image samples. In the test phase, the DnCNN denoises the BM3D processed images using the trained model and generates the denoised image as the final prediction result.

The BM3D algorithm consists of two stages: the basic estimation stage and the final estimation stage. Each stage contains three parts: block matching, collaborative filtering and aggregation. The algorithm contains a large number of parameters, and different parameter values will have a greater influence on the effectiveness of the algorithm, especially the search window size, the search radius, the sliding step size, the number of similar blocks and the threshold parameters, among which the threshold parameters include the size of the similarity threshold and the hard threshold filtering parameters. After combining the DnCNN, it is necessary to re-evaluate all the parameters, and to balance the relationship between detail preservation and noise reduction by adjusting the parameters, so as to better suit the needs of the subsequent processing of the DnCNN to achieve better image

quality. The network structure designed in this paper is shown in Fig.4, with a network depth of 17. The network architecture consists of three parts: convolutional layer (Conv), activation function (PReLU) and batch normalization (BN), which is described as follows:

Layer 1: Conv+PReLU, a filter consisting of 64 convolution kernels with a size of 3×3×1 is used to generate the 64 feature mappings, and the PReLU activation function is used to realize nonlinear feature mapping with a step size of 1×1.

Layers 2-16: Conv+BN+PReLU, a filter consisting of 64 convolution kernels with a size of 3×3×64 is used to generate the 64 feature mappings, and the PReLU activation function is used with a step size of 1×1.

Layer 17: Conv, a filter with a size of 3×3×64 is used for network reconstruction with a step size is 1×1. The network is trained using the residual learning strategy, and finally the denoised image is output.

In the network structure, the 0-padding is adopted to keep the size of the convolution feature map constant at each layer to avoid boundary artifacts.

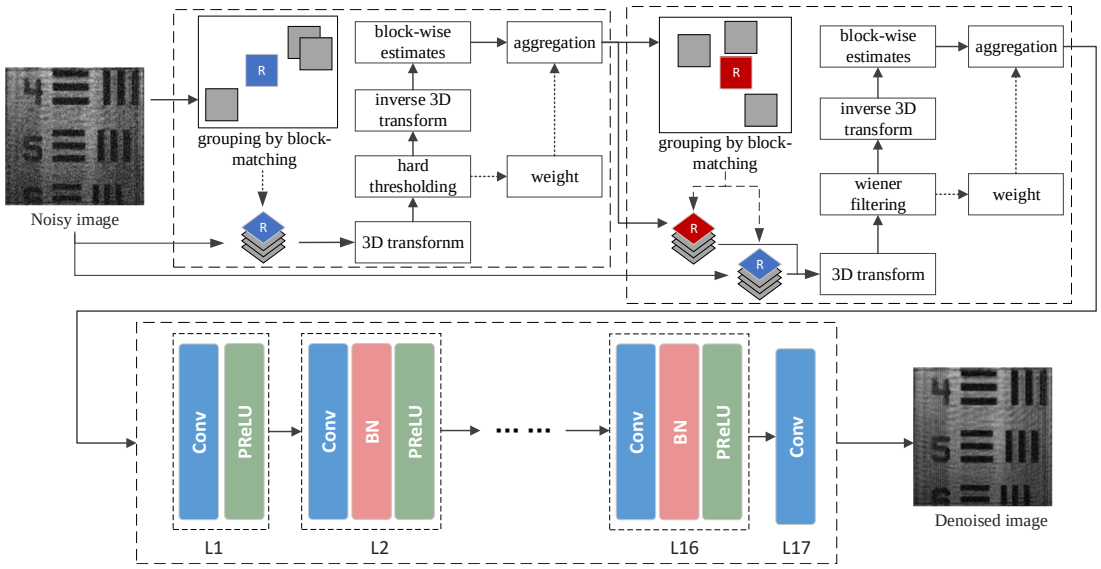

Fig.4. Schematic structure of the improved convolutional neural network based on BM3D.

In this method, because the BM3D has already pre-processed the image and preliminarily reduced the noise, the image input to DnCNN contains less noise. Therefore, DnCNN uses its powerful deep learning capability to further refine denoising based on preserving the fine structure and texture of the image, significantly improving the image quality and reducing the computational complexity. By combining BM3D and DnCNN, the BM3D algorithm can be fully utilized for modelling and denoising the similarity and important statistical information of blocks. Meanwhile, the powerful learning capability of DnCNN can be used to improve the image quality by better removing noise while preserving image detail and structure.

3.2 Activation and Loss Functions

The standard DnCNN usually uses the ReLU function [24] as the network activation function, but there is a hard saturation of zero in the negative semiaxis of the ReLU, which may lead to neuron necrosis and also makes the mean value of the data distribution non-zero. Therefore, PReLU is chosen as the activation function in this paper, whose mathematical expression is:

$$PReLU = \begin{cases} x_i, & x \geq 0 \\ a_i x_i, & x < 0 \end{cases} \tag{4}$$

The PReLU activation function is an improvement on the ReLU. The less than zero part retains more information about the features of the input data, and the parameters are automatically adjusted according to the training to avoid neuron necrosis.

The input to DnCNN is a noisy observation $y = x + v$. During training, the network adopts residual learning to train the residual mapping $R(y; \Theta) \approx v$ which predicts the potential noise-free image $x = y - R(y)$ by learning the mapping function. The mean square error (MSE) between the desired residual image and the image estimated from noise input is:

$$\ell(\Theta) = \frac{1}{2N} \sum_{i=1}^{N} \|R(y_i; \Theta) - (y_i - x_i)\|_F^2 \tag{5}$$

where $y_i - x_i$, $(i = 1,2, \dots, N)$ denotes N training samples containing real noise data, $R(y_i; \Theta)$, $(i = 1,2, \dots, N)$ is N noise data generated by the network through learning, and $\|\cdot\|_F^2$ is the Frobenius norm. During the training process of network, the parameter of the network Θ is optimized by minimizing the MSE between the residual image and the noise input estimation image, and the parameters of the filter are progressively optimized to make $\ell(\Theta)$ as small as possible and $R(y_i; \Theta)$ as close to v as possible, so as to better learn the features of the data.

4 Experimental Verification

In the proposed method, the parameters for BM3D are set as follows: the search window size is 8×8 with a sliding step of 3 and a search radius of 39; the maximum number of similar blocks in the basic estimation is 16 with a similarity threshold size of 3000 and a hard-threshold filtering parameter of 2.7; the maximum number of similar blocks in the final estimation is 32 with a similarity threshold size of 400 and a hard-threshold filtering parameter of 2.0. The batch processing parameters of the neural network are set to 128 with an initial learning rate of 0.0001; using the MultiStepLR scheduler, the learning rate is reduced by 0.5 times at specified milestones to achieve a gradual halving strategy, and the number of training cycles is set to 100. The dataset consists of 2500 training samples for digital holograms, and the holograms collected from the experiments are used as the test samples. All the simulations and experiments in this paper are completed on a computer with a 13th Gen Intel (R) Core (TM) i9-13900 KF CPU, 32G RAM memory and a NVIDIA GeForce RTX 4090 GPU. The Python 3.7 programming language and the Pytorch 2.1 framework are used to train and test the neural network models for the proposed method, DnCNN and CBDNet, under the PyCharm integrated development environment. The simulated dataset preparation, BM3D and Wiener filtering algorithms are implemented using MATLAB 2020b.

4.1 Dataset Preparation

To train the improved convolutional neural network model proposed in this paper, a dataset consisting of simulated images and real images is constructed. The simulated image uses 1000 images from WaterLoo [25] and 1000 images from MIT-Adobe FiveK [26], which are converted into grayscale images. According to the given gray image file of the object, the wavelength of the illumination light, the diffraction distance and the physical width of the CCD, the physical width of the initial plane and the observation plane are not consistent when using the S-FFT to calculate the Fresnel diffraction integral. After the projection width of the object and the width of the CCD array are given, a digital

hologram is formed by using the S-FFT calculation of the Fresnel diffraction integral, and the digital hologram is reproduced to obtain the reconstructed image. The simulation results are shown in Fig.5.

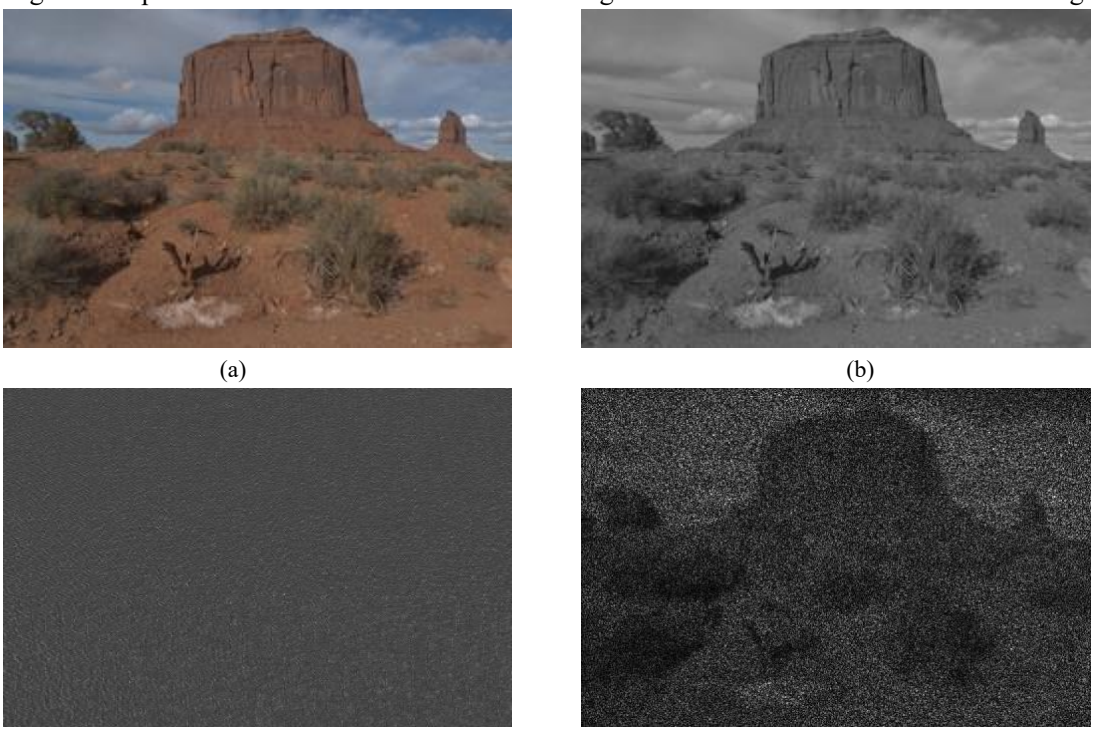

Fig. 5. The simulated results. (a) original image; (b) grayscale image; (c) hologram; (d) reconstructed image.

In this paper, a reflective off-axis digital holographic optical path system is constructed, as shown in Fig.6. A He-Ne laser with a wavelength of 632.8 nm is used as the light source. The beam emitted from the laser light source is reflected by the reflectors M1 and M2, and then is processed by the beam expander (BE) collimator. It is reflected by the right-angle reflector R to the beam splitter (BS), and then split into two beams at a ratio of 1:1. One beam is modulated by the test sample as the object light, and the other beam is reflected by the reflector M3 as the reference light. The angle between the object light and the reference light is 5°. Finally, the object light interferes with the reference light to form a hologram, which is recorded by the CCD camera. The experimental setup is shown in Fig.7. 100 digital holograms of test samples were acquired by the above experimental setup, and their reconstructed images were obtained by using the Fresnel diffraction method. Then, the random noise in the range of [0,50] was added to them to the reconstructed images with different level noises. Wiener filtering was performed on the reconstructed image obtained by the experiment. By adjusting the parameters of the filter, different levels of noise reduction were achieved, and the new reconstructed images were generated. After the above processing, 500 reconstructed images were finally obtained as real images, and together with the simulated images, formed the dataset used in this paper.

In the experiments, 150 images were randomly selected from the real image dataset of the non-training set as the test sample set, and two representative images were carefully selected from this set as typical cases for further analysis. The dataset containing 2500 samples is used for model training and optimization. In addition, to improve the generalization ability of the model, a data augmentation strategy is adopted to simulate different perspectives and postures, i.e., when loading the training data, a rotation operation with a range of -90~°90° is randomly applied. This strategy not only effectively increases the number of training samples, but also significantly improves the robustness of the model, allowing it to show a good generalization ability for new samples.

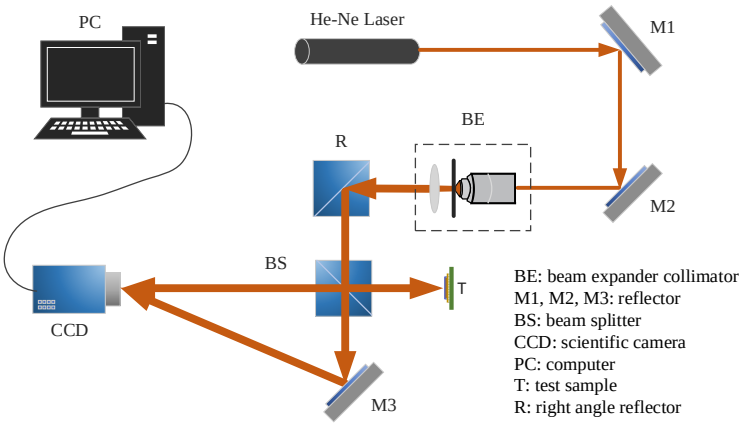

Fig.6. The schematic diagram of system optical path structure.

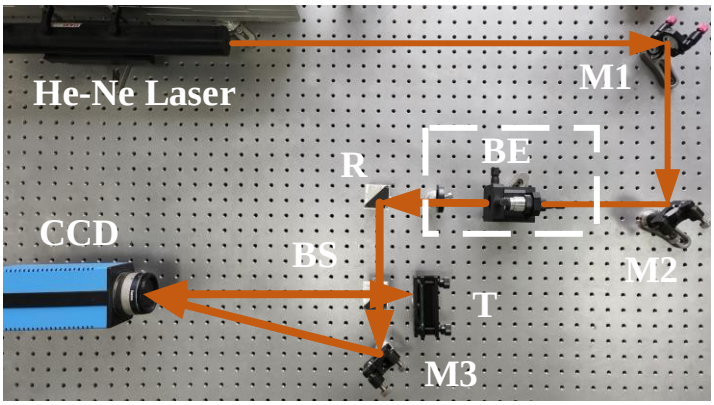

Fig.7. Experimental setup.

4.2 Image Quality Evaluation Metrics

In the research on noise suppression on DH, the evaluation of denoising effect mainly includes qualitative and quantitative analysis, and the quantitative evaluation method is to evaluate the image quality based on the mathematical models. Peak signal-to-noise ratio (PSNR) [27], structural similarity index (SSIM) [28], equivalent number of looks (ENL) [29], speckle suppression index (SSI) [30] and speckle suppression and mean preservation index (SMPI) [31] are used to evaluate the image quality after noise reduction.

（1）PSNR

$$MSE = \frac{1}{H \times W} \sum_{i=0}^{H-1} \sum_{j=0}^{W-1} [g(i,j) - I(i,j)]^2 \tag{6}$$

$$PSNR = 10log_{10}\left(\frac{(2^n - 1)^2}{MSE}\right) \tag{7}$$

where *MSE* is the mean square error of the denoised image *I* and the noisy image *g*, $I(i,j)$ and $g(i,j)$ are the pixel values at the respective coordinates, *H* and *W* are the height and width of the image, respectively, and *n* is the number of bits per pixel, which is generally assumed to be 8, i.e., the number of pixel gray levels is 256. PSNR is measured in dB, and the larger the value, the lower the distortion.

（2）SSIM

$$SSIM = \frac{(2\mu_I\mu_g + C_1)(2\sigma_{Ig} + C_2)}{(\mu_I^2 + \mu_g^2 + C_1)(\sigma_I^2 + \sigma_g^2 + C_2)} \tag{8}$$

where μ is the mean value of the image, σ is the standard deviation of the image, C_1 and C_2 are small

constants to ensure that the denominator is non-zero, respectively. SSIM evaluates the image quality from three aspects of image brightness, contrast and structure. The mean is used to estimate the brightness, the standard deviation is used to estimate the contrast, and the covariance is used as the measure of structural similarity. Compared with other metrics, SSIM is much closer to the results of subjective evaluation. The higher the SSIM value, the more detailed information, and the higher the image quality.

（3）ENL

$$ENL = \left(\frac{\mu_I}{\sigma_I}\right)^2 \tag{9}$$

where μ_I and σ_I are the mean value and standard deviation of the image, respectively. ENL is usually used to measure the performance of different noise reduction filters. When the ENL value is larger, it indicates that the image is smoother, which means there are fewer noise spurs in the image, and the noise reduction performance of the filter is better.

（4）SSI

$$SSI = \frac{\sqrt{\sigma(I)}}{\mu(I)} \frac{\mu(g)}{\sqrt{\sigma(g)}} \tag{10}$$

The SSI reflects the speckle suppression ability of the algorithm, whose value is usually less than 1. The smaller the value, the better the speckle suppression performance.

（5）SMPI

$$SMPI = \left[1 + \left|\mu_g - \mu_I\right|\right] * \frac{\sqrt{\sigma_I}}{\sqrt{\mu_g}} \tag{11}$$

In the process of noise reduction, SSI may be unreliable if the mean value in the denoised image differs greatly from the mean value of the original image. And SMPI can be better used to evaluate the noise reduction performance of the algorithm. Theoretically, the smaller the value of SMPI, the better the noise reduction performance.

4.3 Experimental Results and Analysis

The holograms of coins and optical resolution plates were collected by the above experimental setup, as shown in Fig.8. The proposed method is validated by comparing the noise reduction results with those of Wiener filtering, BM3D [27], DnCNN [18] and CBDnet [32].

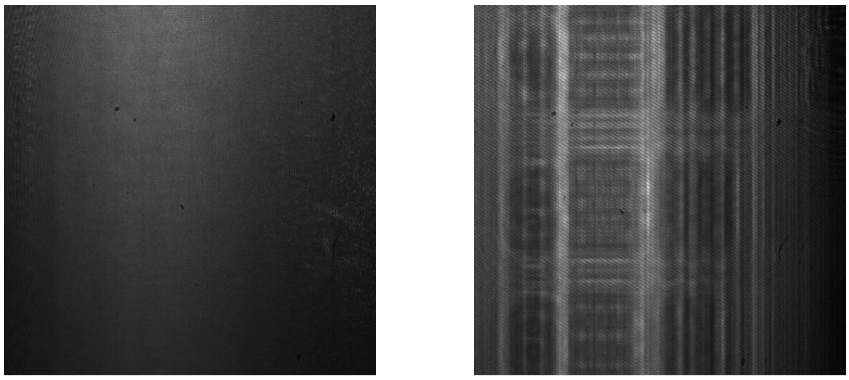

(a) (b)

Fig.8. Hologram. (a) coin; (b) optical resolution plate.

4.3.1 Analysis of Noise Reduction Results for Coin Reconstructed Image

The hologram shown in Fig.8 (a) is reconstructed by Fresnel diffraction with a reconstruction distance of 800 mm, and the reconstructed image is shown in Fig.9 (a), which is denoised by the above five methods, respectively. The experimental results are shown in Fig.9 (b-f). As can be clearly shown

from Fig.9, the proposed method significantly improves the image clarity compared to other methods, making the objects and contours in the image more distinct. It not only effectively removes the noise, but also enhances the image contrast. In order to quantitatively analyze the noise reduction effect of various methods, the above five metrics are used to evaluate the image quality of reconstruction after noise reduction, and the calculation results are shown in Fig.10.

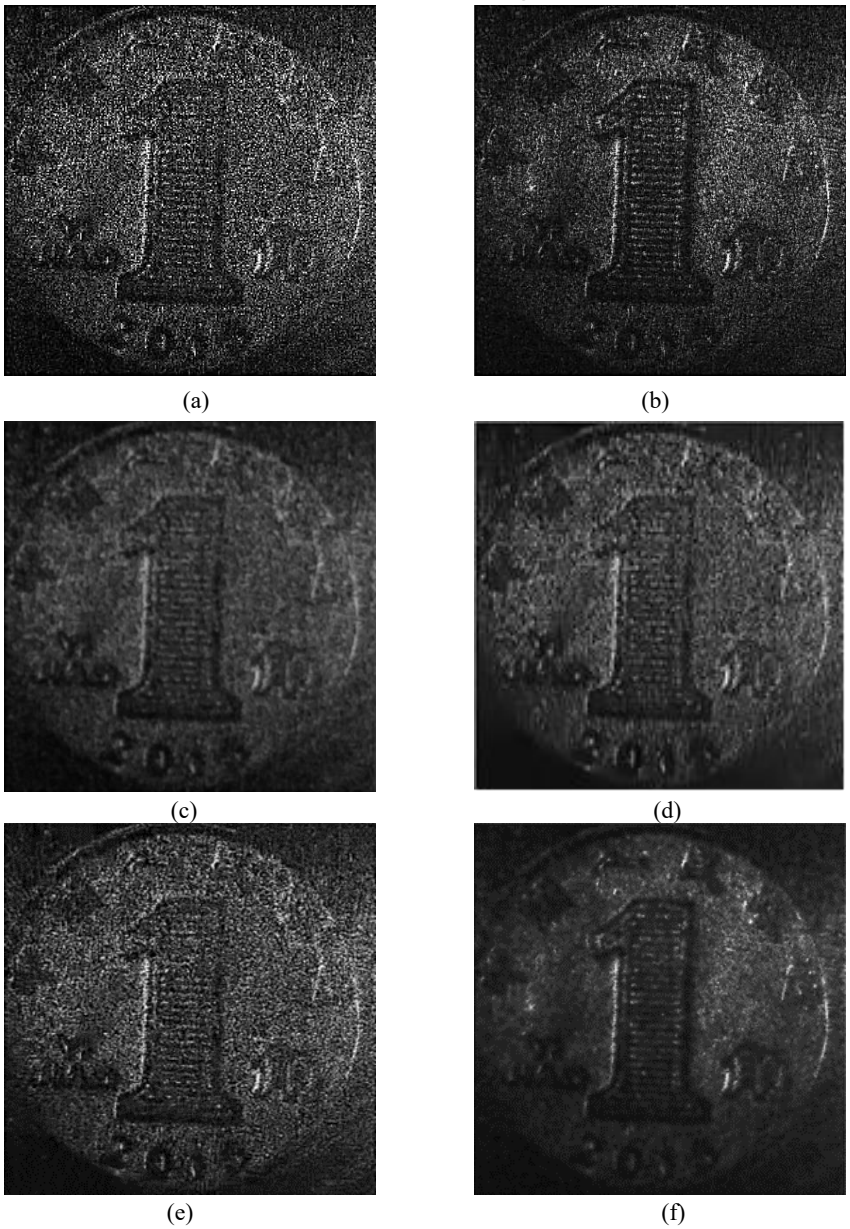

Fig.9. Noise reduction results of different methods for coin reconstructed image. (a) reconstructed image; (b) the proposed method; (c) CBDNet; (d) DnCNN; (e) BM3D; (f) Wiener filtering.

It can be observed from Fig.10 that compared with the other four methods, the values of PSNR, SSIM and ENL corresponding to the image denoised by the proposed method were the largest, while the values of SSI and SMPI were the smallest. However, it should be noted that the computational time of the proposed method was slightly longer than that of the other four methods. Therefore, the proposed method is superior to the other four methods in terms of noise reduction performance and image detail preservation, and the trained convolutional neural network can capture the invalid noise component of the hologram and preserve the detailed information of the target image.

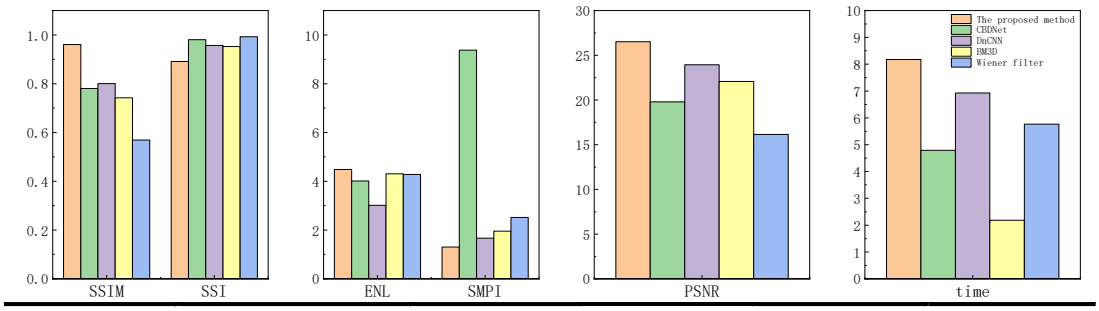

	The proposed method	CBDNet	DnCNN	BM3D	Wiener filter
SSIM	**0.9610**	0.7805	0.8005	0.7425	0.5694
PSNR	**26.5212**	19.7960	23.9437	22.0816	16.1422
ENL	**4.4830**	4.0118	3.0163	4.3073	4.2787
SSI	**0.8913**	0.9803	0.9567	0.9523	0.9924
SMPI	**1.3061**	9.3751	1.6654	1.9543	2.5182
time/s	**8.1746**	4.7893	6.9267	2.1828	5.7648

Fig.10. Calculation results of five metrics for Fig.9 (b-f).

4.3.2 Analysis of Noise Reduction Results of the Reconstructed Image for Optical Resolution Plate

To further validate the proposed method, the hologram shown in Fig.8 (b) is reconstructed using Fresnel diffraction with a reconstruction distance of 600 mm, and the reconstructed image is shown in Fig.11 (a), which is denoised using the same five methods mentioned above, respectively. The experimental results are shown in Fig.11 (b-f). It can be seen from Fig.11 that the proposed method achieved a better denoising performance compared to other methods. To quantitatively assess the denoising performance of various methods, the above five metrics are used to evaluate the quality of the reconstructed image after noise reduction, and the calculation results are shown in Fig.12.

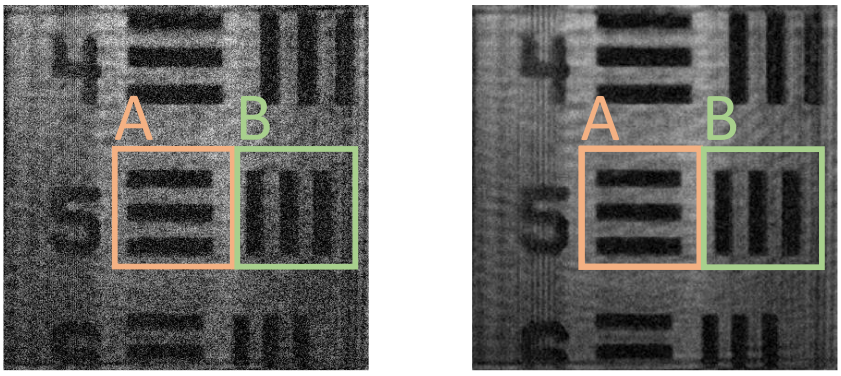

(a) (b)

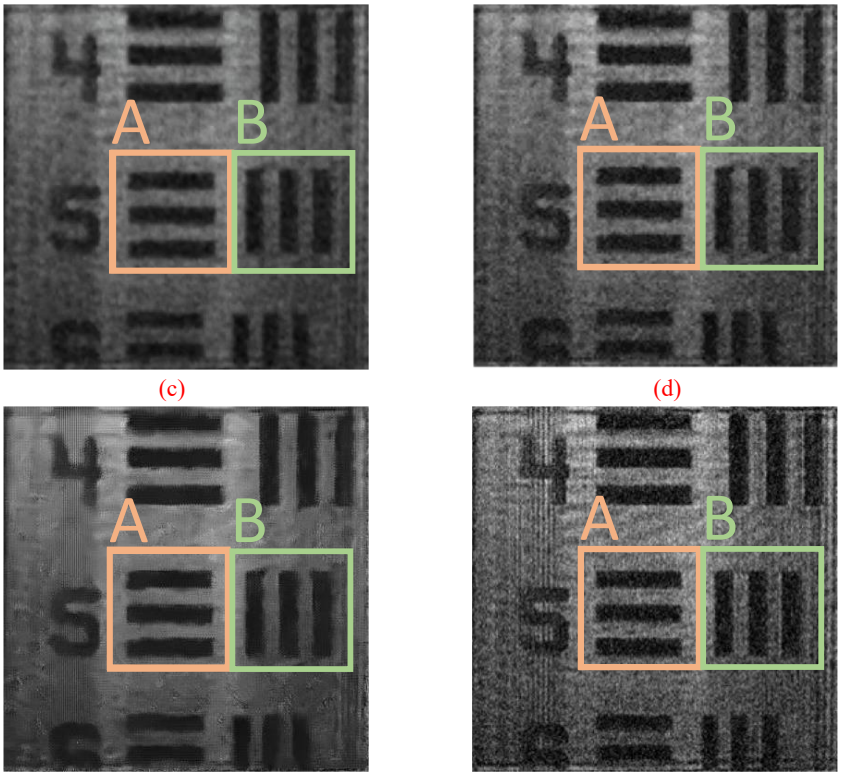

(c) (d)

(e) (f)

Fig.11. Noise reduction results of different methods of reconstructed image for optical resolution plate. (a) reconstructed image; (b) the proposed method; (c) CBDNet; (d) DnCNN; (e) BM3D; (f) Wiener filtering.

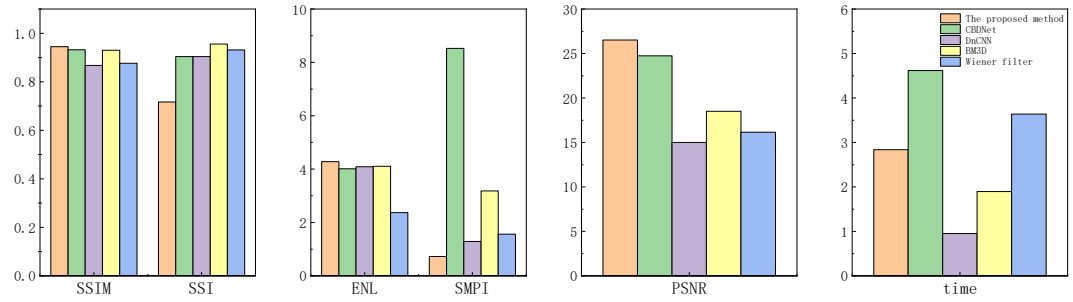

	The proposed method	CBDNet	DnCNN	BM3D	Wiener filter
SSIM	**0.9450**	0.9323	0.8672	0.9298	0.8764
PSNR	**26.5172**	24.7332	15.0059	18.5050	16.1435
ENL	**4.2795**	4.0112	4.0875	4.1037	2.3689
SSI	**0.7165**	0.9038	0.9036	0.9559	0.9313
SMPI	**0.7231**	8.5245	1.2919	3.1813	1.5627
time/s	**2.8359**	4.6174	0.9528	1.8968	3.6378

Fig.12. Calculation results of five metrics for Fig.11 (b-f).

As can be shown from Fig.12, the PSNR, SSIM and ENL of the denoised image after by the proposed method had the largest values, while SSI and SMPI had the smallest values. In addition, the computational time of the proposed method was significantly shorter than that of CBDNet and Wiener filtering, but longer than other methods. Thus, the final conclusion was consistent with the results of

the previous experimental results, which further demonstrated the practicability and effectiveness of the proposed method.

To better evaluate the local quality of the reconstructed image after noise reduction, a typical region *A* and *B* in Fig.11 are selected to amplify as shown in Figs.13 and 14. The above five metrics are used to evaluate the performance on noise reduction and detail preservation, and the calculation results are shown in Figs.15 and 16.

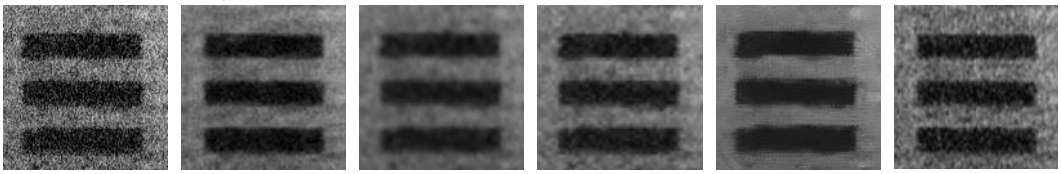

(a) (b) (c) (d) (e) (f)

Fig.13. Comparison of results for region *A* in Fig.10. (a) reconstructed image; (b) the proposed method; (c) CBDNet; (d) DnCNN; (e) BM3D; (f) Wiener filtering.

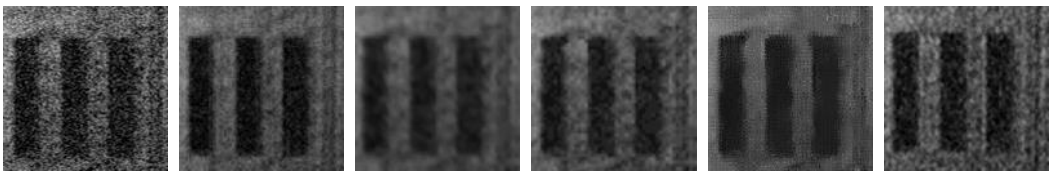

(a) (b) (c) (d) (e) (f)

Fig.14. Comparison of results for region B in Fig.10. (a) reconstructed image; (b) the proposed method; (c) CBDNet; (d) DnCNN; (e) BM3D; (f) Wiener filtering.

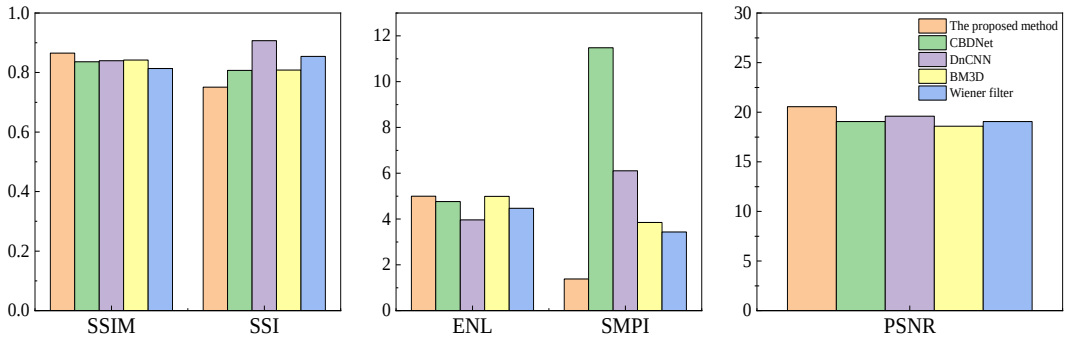

	The proposed method	CBDNet	DnCNN	BM3D	Wiener filter
SSIM	**0.8653**	0.8361	0.8399	0.8422	0.8134
PSNR	**20.5650**	19.0540	19.6056	18.5925	19.0574
ENL	**4.9998**	4.7617	3.9606	4.9869	4.4668
SSI	**0.7506**	0.8072	0.9069	0.8082	0.8540
SMPI	**1.3820**	11.4804	6.1092	3.8503	3.4365

Fig.15. Calculation results of five metrics for Fig.13 (b-f).

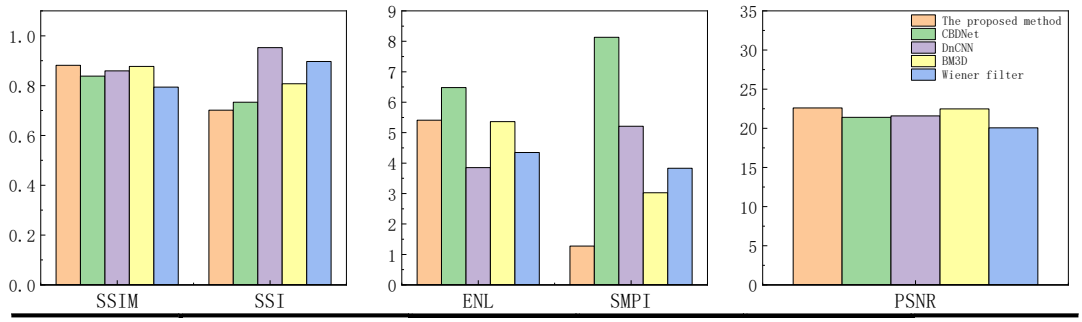

	The proposed method	CBDNet	DnCNN	BM3D	Wiener filter
SSIM	**0.8817**	0.8382	0.8590	0.8769	0.7943
PSNR	**22.6053**	21.4115	21.5849	22.4703	20.0661
ENL	**5.4115**	6.4783	3.8529	5.3615	4.3460
SSI	**0.7014**	0.7333	0.9527	0.8076	0.8970
SMPI	**1.2734**	8.1304	5.2089	3.0266	3.8285

Fig.16. Calculation results of five metrics for Fig.14 (b-f).

From Figs.13-16, it can be concluded that the proposed method achieved a better performance on noise reduction and detail preservation than the other four methods.

5 Conclusions

In this paper, we proposed an improved convolutional neural network noise reduction method based on BM3D. First, the similarity and important statistical information between blocks were obtained by BM3D. Then, the optimized DnCNN was used to learn the relationship between noise and noisy images for a large number of samples using a dataset for holographic reconstruction images generated by the simulation and experimental acquisition methods, thus achieving more accurate and comprehensive processing for the complex noise patterns in the images to improve image clarity and preserve more image details. Noise reduction experiments were performed on the noisy reconstructed images using the proposed with Wiener filtering, BM3D, DnCNN and CBDnet, respectively. Five metrics were adopted to quantitatively evaluate the image quality after noise reduction.

Experimental results showed that the proposed method is significantly better than the other four methods in terms of noise reduction performance and detail retention, which effectively improves the noise reduction effect and the quality of reconstructed image. Although its computational time is slightly longer than other methods, which increases by about a few seconds, this small-time cost brings more excellent image processing effect. Overall, this method achieves a good balance between efficiency and effect. Aiming at the common noise problem in optical microscopy imaging, this method can enhance the accuracy of microstructure observation and analysis by improving the signal-to-noise ratio. In the field of optical interferometry and holographic imaging, this method can effectively solve the image distortion and blurring caused by noise. By suppressing noise generation or denoising in the reconstruction process, the clarity and authenticity of the reconstructed image are ensured, which is of great importance in the above research fields.

Funding. National Natural Science Foundation of China (Grant No. 52175518), Natural Science Basic Research Program of Shaanxi Province (Program No. 2019JQ-791), Scientific Research Program Funded by Shaanxi Provincial Education Department (Program No. 21JK0769).

Disclosures. The authors declare no conflicts of interest.

Data availability. Data underlying the results presented in this paper are not publicly available at this time but may be obtained from the authors upon reasonable request.

References

[1] Song H Y, Li J N, Fan L L, et al. Study on collinear holographic storage system with orthogonal phase encryption[J]. Chinese Journal of Lasers,2023,50(18):229-236.

[2] Marquet P, Depeursinge C, Magistretti P J. Review of quantitative phase-digital holographic microscopy: promising novel imaging technique to resolve neuronal network activity and identify cellular biomarkers of psychiatric disorders[J]. Neurophotonics, 2014, 1(2): 020901-020901.

[3] Anne M, Moritz K E, Álvaro B, et al. Interlaboratory evaluation of a digital holographic microscopy-based assay for label-free in vitro cytotoxicity testing of polymeric nanocarriers[J]. Drug Delivery and Translational Research, 2022, 12(9): 2207-2224.

[4] Turko N A, Eravuchira P J, Barnea I, et al. Simultaneous three-wavelength unwrapping using external digital holographic multiplexing module[J]. Optics Letters, 2018, 43(9): 1943-1946.

[5] Chen Y H, Cai Y J. Laser coherence modulation and its applications[J]. Acta Optica Sinica, 2016,36(10):26-42.

[6] Xu L H, Wang Y F, Jia Yu F, et al. Research progress of low-coherence laser[J]. Acta Optica Sinica, 2021,41(08): 110-123.

[7] Hao Y, Asundi A. Impact of charge-coupled device size on axial measurement error in digital holographic system[J]. Optics Letters,2013,38(8):1194-1196.

[8] Juptner W, Schnars U. Direct recording of holograms by a CCD target and numerical reconstruction[J]. Applied Optics,1994,33(2):179-181.

[9] Dubois F, Requena M L N, Minetti C, et al. Partial spatial coherence effects in digital holographic microscopy with a laser source[J]. Applied optics, 2004, 43(5): 1131-1139.

[10] Gong Q, Qin Y. LED-based digital holography[J], Journal of Applied Optics, 2010,31(02):237-241.

[11] Rosen J, Brooker G. Digital spatially incoherent Fresnel holography[J]. Optics Letters, 2007,32(8):912-914.

[12] Chen K, Chen L, Xiao J Q, et al. Reduction of speckle noise in digital holography using a neighborhood filter based on multiple sub-reconstructed images[J]. Optics Express, 2022, 30(6): 9222-9232.

[13] Bianco V, Paturzo M, Memmolo P, et al. Random resampling masks: a non-Bayesian one-shot strategy for noise reduction in digital holography[J]. Optics Letters, 2013, 38(5): 619-621.

[14] Chen Y, Liu D, Liang S, et al. Noise suppression in the reconstructed image of digital holography based on BEMDV method using improved PSO[J]. Applied Optics, 2023, 62(19): 5159-5169.

[15] Choi G, Ryu D H, Jo Y J, et al. Cycle-consistent deep learning approach to coherent noise reduction in optical diffraction tomography[J]. Optics express, 2019, 27(4): 4927-4943.

[16] Chen L, Chen X, Cui H, et al. Image enhancement in lensless inline holographic microscope by inter-modality learning with denoising convolutional neural network[J]. Optics Communications, 2021, 484: 126682.

[17] Fang Q, Xia H, Song Q, et al. Speckle denoising based on deep learning via a conditional generative adversarial network in digital holographic interferometry[J]. Optics Express, 2022, 30(12): 20666-20683.

[18] Smita R T, Narayan R Y, Lalita G. PReLU and edge-aware filter-based image denoiser using convolutional neural network[J]. IET Image Processing,2020,14(15):3869-3879.

[19] Zhou W J, Zou S, He D K, et al. Speckle noise reduction of holograms based on spectral convolutional neural network[J]. Acta Optica Sinica, 2020,40(05):67-74.

[20] Zhang K, Zuo W, Chen Y, et al. Beyond a gaussian denoiser: Residual learning of deep CNN for image denoising[J]. IEEE Transactions on Image Processing, 2017, 26(7): 3142-3155.

[21] Yan F, Yan H, Yu Y, et al. The suppression of phase error by applying window functions to digital holography[J]. Optics and Lasers in Engineering, 2016, 86: 206-215.

[22] Zhan X, Gan C, Ding Y, et al. Speckle noise suppression based on empirical mode decomposition and improved anisotropic diffusion equation[C]. Photonics, 2022, 9(9): 611.

[23] Bianco V, Memmolo P, Leo M, et al. Strategies for reducing speckle noise in digital holography[J]. Light: Science & Applications, 2018, 7(1): 48.

[24] Wang G., Giannakis B. G., and Chen J. Learning ReLU Networks on Linearly Separable Data: Algorithm, Optimality, and Generalization[J]. IEEE Transactions on Signal Processing, 2019, 67(09): 2357-2370.

[25] Kede Ma, Zhengfang Duanmu, Qingbo Wu, Zhou Wang, Hongwei Yong, Hongliang Li, and Lei Zhang. Waterloo exploration database: New challenges for image quality assessment models[J]. Transactions on Image Processing, 2016:1004–1016.

[26] Vladimir Bychkovsky, Sylvain Paris, Eric Chan, and Fredo Durand. Learning photographic global tonal adjustment with a database of input/output image pairs [C]. IEEE Conference on Computer Vision and Pattern Recognition, 2011.

[27] Cheremkhin P A, Kurbatova E A. Comparative appraisal of global and local thresholding methods for binarisation of off-axis digital holograms[J]. Optics and Lasers in Engineering, 2019, 115: 119-130.

[28] Cheremkhin P A, Evtikhiev N N, Kozlov A V, et al. An optical-digital method of noise suppression in digital holography[J]. Journal of Optics, 2022, 24(11): 115702.

[29] Tounsi Y, Kumar M, Kaur K, et al. Speckle-noise filtering based on non-local mean sparse principal component analysis method[J]. Optics and Lasers in Engineering, 2023, 164: 107507.

[30] Chen P, Cai X W, Zhao D D, et al. Despeckling for side-scan sonar images based on adaptive block-matching and 3D filtering[J]. Opto-Electronic Engineering, 2020,47(07):71-80.

[31] Singh P, Diwakar M, Singh V, et al. A new local structural similarity fusion-based thresholding method for homomorphic ultrasound image despeckling in NSCT domain[J]. Journal of King Saud University-Computer and Information Sciences, 2023, 35(7): 101607.

[32] Guo S, Yan Z, Zhang K, et al. Toward convolutional blind denoising of real photographs[C]. Proceedings of the IEEE Conference on Computer Vision and Pattern Recognition, 2019: 1712-1722.